Journal of Sound and Vibration 329 (2010) 4740–4755

Contents lists available at ScienceDirect

Journal of Sound and Vibration

journal homepage: www.elsevier.com/locate/jsvi

Effectiveness of T-shaped acoustic resonators in low-frequency sound transmission control of a finite double-panel partition

Deyu Li [a], Xiao-Hong Zhang [b], Li Cheng [a,*], Ganghua Yu [a]

[a] Department of Mechanical Engineering, The Hong Kong Polytechnic University, Hung Home, Kowloon, Hong Kong SAR, China
[b] Department of Mathematics and Physics, North China Electric Power University, China

ARTICLE INFO

Article history:
Received 8 April 2009
Received in revised form
17 May 2010
Accepted 18 May 2010
Handling Editor: R.E. Musafir
Available online 18 June 2010

ABSTRACT

Double-panel partitions are widely used for sound insulation purposes. Their insulation efficiency is, however, deteriorated at low frequencies due to the structural and acoustic resonances. To tackle this problem, this paper proposes the use of long T-shaped acoustic resonators in a double-panel partition embedded along the edges. In order to facilitate the design and assess the performance of the structure, a general vibro-acoustic model, characterizing the interaction between the panels, air cavity, and integrated acoustic resonators, is developed. The effectiveness of the technique as well as the optimal locations of the acoustic resonators is examined at various frequencies where the system exhibits different coupling characteristics. The measured optimal locations are also compared with the predicted ones to verify the developed theory. Finally, the performance of the acoustic resonators in broadband sound transmission control is demonstrated.

1. Introduction

Double-panel partitions comprising an air cavity between two parallel plates are widely used in building, vehicle, and aerospace structures because of their light weight and high transmission loss. However, the sound isolation efficiency of double-panel partitions deteriorates at low frequencies due to the plate–air–plate resonances. Therefore, there has been a persistent effort in developing new ideas and solutions to improve the sound insulation capability of double partitions as evidenced by a large amount of existing work in the literature. Typical examples include adjusting panel thickness [1,2], reducing power flow path [3], using passive acoustic devices [4–6], and using active noise and active structural–acoustic control methods [7–9]. In passive treatment, Mason and Fahy [4] utilized classical Helmholtz resonators (HR) to shunt the stiffness of the air cavity to improve the insulation performance of fuselage walls for an aircraft in the mass–air–mass frequency of the partition. Li and Vipperman [5] developed a long T-shaped acoustic resonator (TAR) in the sound transmission control of an expendable launch vehicle (ELV) payload fairing. The potential of such technology has been successfully demonstrated in a relatively broad frequency band [6]. In the present paper, TARs are used to control the low-frequency sound transmission of double-panel partitions, with particular attention paid to the development of a simulation model and the assessment of the effectiveness of this technique.

Various analysis tools for sound transmission through double-panel partitions have previously been proposed. Early work can be traced back to London [10], who discussed the sound transmission through double-panel partitions consisting

* Corresponding author. Tel.: +852 2766 6769; fax: +852 2365 4703.
E-mail address: mmlcheng@polyu.edu.hk (L. Cheng).

0022-460X/$ - see front matter
doi:10.1016/j.jsv.2010.05.020

of two identical walls coupled by an air space. Since then, the topic has received a great deal of attention. Series of numerical techniques, such as statistical energy analysis [11], finite element approach [12], and path-mobility method [13], have been used for the prediction of sound transmission. However, few developments are related to the sound transmission control using acoustic resonators. Sound transmission through an infinite double-panel partition with HRs was studied by Mason and Fahy [4]. Their work only targeted the mass–air–mass resonance since flexible modes of both cavity and panels were not presented in their model. In an effort to develop a vibro-acoustic model for the sound transmission control of a cylindrical structure, dynamic vibration absorbers (DVA) and HRs were simultaneously used by Estève and Johnson [14,15]. Their work focused on examining the ability and robustness of the combined DVA/HR treatment. Recently, a vibro-acoustic model for a double-panel partition with HRs was developed by Mao and Pietrzko [16]. Similarly as done by Mason and Fahy [4], however, only the control at the mass–air–mass resonance was examined, and no further detailed analysis and experimental verification were presented. More recent research on acoustic coupling between an enclosure and an acoustic resonator array has shown that the control performance of acoustic resonators strongly depends on their location and the characteristics of the cavity [17]. This location-dependence is likely to be increased in the double partition configuration, which exhibits complex vibro-acoustic interaction among the panels, the air cavity, and the integrated long TARs. This reality imposes a need for developing reliable modeling tools to guide the design and to predict control performance.

In this paper, a general vibro-acoustic model is developed for double-panel partitions with embedded TARs. The model takes into account the structural and acoustic interaction among the panels, air cavity, and acoustic resonators. Upon classifying dominant dips in the transmission loss curve corresponding to a strong sound transmission, attempts are made to examine the effectiveness of TARs at different frequencies exhibiting different coupling characteristics. The optimal location of TARs is determined and compared with experimentally measured ones to verify the development. Broadband sound transmission control at low frequencies using multiple TARs is also numerically demonstrated.

2. Theory

Fig. 1(a) shows the system under investigation. A double-panel partition, having two parallel panels ($L_x \times L_y$) and one air cavity ($L_x \times L_y \times h$), is surrounded by an infinite baffled wall. The panel at the top is denoted as *incidence panel* and the one at the bottom is referred to as *radiation panel*. A TAR consists of three branches indicated in Fig. 1(b), which can be easily integrated into the partition along the rigid boundaries of the air cavity due to its large aspect ratio. TARs are modeled as point sound sources. It is assumed that the normal displacement of the incidence panel $w^I(x,y,t)$ is positive inward, and that of the radiation panel $w^R(x,y,t)$ and the source volume velocity $q_m(x_m^T,y_m^T,z_m^T,t)$ of the mth TAR located at (x_m^T,y_m^T,z_m^T) is positive outward. The time dependence is assumed throughout as $e^{-i\omega t}$. The superscripts C, I, R, and T refer to cavity, incidence panel, radiation panel, and T-shaped acoustic resonator, respectively.

The bending equations of the panels subjected to an incident wave $p^{IN}(x,y,z^I,t)$ can be written as

For the incidence panel:

$$D^I\nabla^4 w^I(x,y,t)+m^I\ddot{w}^I(x,y,t)=2p^{IN}(x,y,z^I,t)-p(x,y,z^I,t), \tag{1}$$

For the radiation panel:

$$D^R\nabla^4 w^R(x,y,t)+m^R\ddot{w}^R(x,y,t)=p(x,y,z^R,t), \tag{2}$$

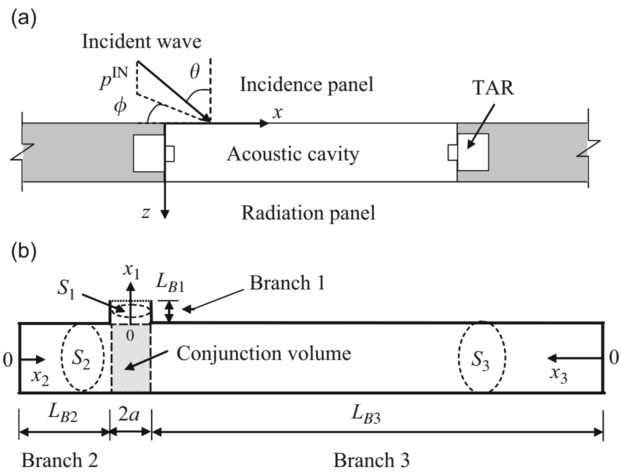

Fig. 1. (a) Baffled double-panel partition and (b) long T-shaped acoustic resonator.

where m^I and m^R are the area density of the incidence and radiation panels, respectively; $D{=}h^3E/12(1-\nu^2)$ is the flexural rigidity of the panel; h is the thickness of the panel; E is Young's modulus; ν is Poisson's ratio and $p(x,y,z,t)$ the pressure response in the cavity. In the above equations, the fluid loadings on the outside of both panels are ignored, which is a well-accepted simplification for most cases of light fluid coupling [18].

The wave equation governing the pressure fields inside the air cavity can be expressed as

$$\nabla^2 p(x,y,z,t) - \frac{1}{c^2}\ddot{p}(x,y,z,t) = -\rho_0 \sum_{m=1}^{M} \dot{q}_m(x,y,z,t)\delta(x-x_m^T)\delta(y-y_m^T)\delta(z-z_m^T) - 2\rho_0 \ddot{w}^I(x,y,z,t)\delta(z-z^I) + 2\rho_0 \ddot{w}^R(x,y,z,t)\delta(z-z^R), \tag{3}$$

where $\delta(x-x_0)$ is the Dirac delta function; c the speed of sound; and ρ_0 the air density. In this equation, the source volume velocity $q_m(x,y,z,t)$ of the mth resonator can be represented in terms of the averaged pressure at its aperture and its acoustic impedance Z_m as

$$q_m(x,y,z,t) = \frac{p(x,y,z,t)}{Z_m}.$$

The acoustic impedance Z of the TAR at its external aperture was derived in [5] assuming a harmonic regime as

$$Z = \mathrm{i}z_0 \frac{1-(S_2/S_1)\tan(k_1L_1)\tan(k_2L_2)-(S_3/S_1)\tan(k_1L_1)\tan(k_3L_3)}{S_1\tan(k_1L_1)+S_2\tan(k_2L_2)+S_3\tan(k_3L_3)},$$

where L_j (j=1,2,3) is the effective length of Branch j, which can be estimated using the end corrections proposed in [5]; $z_0{=}c\rho_0$ is the characteristic acoustic impedance of the fluid; k_j is a complex wavenumber when the absorptive process within the fluid and at the walls of the resonator are considered, which is expressed with a dispersion relation in [19] as $k_j{=}k_0-\mathrm{i}\gamma_j$, where $k_0{=}\omega/c$ is the wavenumber and γ_j ($\ll k_0$) is the attenuation coefficient of Branch j defined in [20] and given by

$$\gamma_j = \sqrt{\frac{\omega\mu}{8cz_0}}\left(1+\frac{\chi-1}{\sqrt{P_r}}\right)\frac{L_j^P}{S_j},$$

where μ is the shear viscosity coefficient, χ is the specific heat ratio, $P_r = \mu C_p/\kappa$ is the Prandtl number of air, C_p is the specific heat at constant pressure, κ is the coefficient of thermal conduction, and L_j^P and S_j are the inner perimeter and cross-sectional area of tube j, respectively.

The pressure in the cavity can be expanded in terms of the acoustic modal shape φ_j as

$$p(x,y,z,t) = \sum_{j=1}^{\infty} \varphi_j(x,y,z)P_j e^{-\mathrm{i}\omega t} \tag{4}$$

and the displacement of the panels can be expanded in terms of the structural modal shape ψ_n as

$$w(x,y,t) = \sum_{n=1}^{\infty} \psi_n(x,y)W_n e^{-\mathrm{i}\omega t}, \tag{5}$$

where P_j is the amplitude of the modal pressure response and W_n is the amplitude of the modal displacement response.

Acoustic and structural modal shapes satisfy the following characteristic equations, respectively:

$$\nabla^2\varphi_j(x,y,z) + \left(\frac{\alpha_j}{c}\right)^2 \varphi_j(x,y,z) = 0, \tag{6}$$

$$D^I\nabla^4\psi_n^I(x,y) - m^I(\beta_n^I)^2\psi_n^I(x,y) = 0, \tag{7}$$

$$D^R\nabla^4\psi_n^R(x,y) - m^R(\beta_n^R)^2\psi_n^R(x,y) = 0, \tag{8}$$

where α_j is the jth acoustic natural angular frequency and β_n is the nth structural angular frequency of panels. Substituting Eqs. (4)–(8) into (1)–(3) and applying orthogonality properties of modal shapes yield the following equations:

For the incidence panel:

$$[\omega^2 + \mathrm{i}2\xi_n^I\beta_n^I\omega - (\beta_n^I)^2]M_n^I W_n^I = \sum_{h=1}^{J} C_{h,n}^I P_h - 2P_n^{\mathrm{IN}}, \tag{9}$$

For the radiation panel:

$$[\omega^2 + \mathrm{i}2\xi_n^R\beta_n^R\omega - (\beta_n^R)^2]M_n^R W_n^R = -\sum_{h=1}^{J} C_{h,n}^R P_h, \tag{10}$$

For the cavity:

$$\left[\omega^2+\mathrm{i}2\xi_j^C\alpha_j\omega-\alpha_j^2\right]\frac{\Lambda_j}{\rho_0 c^2}P_j-\mathrm{i}\omega\sum_{h=1}^{J}\left[\sum_{m=1}^{M}\frac{\varphi_j(x_m^T,y_m^T,z_m^T)\varphi_h(x_m^T,y_m^T,z_m^T)}{Z_m}P_h\right]=\omega^2\sum_{n=1}^{N^I}C_{j,n}^I W_n^I-\omega^2\sum_{n=1}^{N^R}C_{j,n}^R W_n^R, \tag{11}$$

where

$$\Lambda_j = iiint;_V[\varphi_j(x,y,z)]^2\,\mathrm{d}x\,\mathrm{d}y\,\mathrm{d}z,$$

$$M_n = m\iint_S[\psi_n(x,y)]^2\,\mathrm{d}x\,\mathrm{d}y,$$

$$P_n^{\mathrm{IN}} = \iint_S p^{\mathrm{IN}}(x,y,z^I)\psi_n^I(x,y)\,\mathrm{d}x\,\mathrm{d}y,$$

$$C_{j,n}^I = \iint_S \varphi_j(x,y,z^I)\psi_n^I(x,y)\,\mathrm{d}x\,\mathrm{d}y,$$

$$C_{j,n}^R = \iint_S \varphi_j(x,y,z^R)\psi_n^R(x,y)\,\mathrm{d}x\,\mathrm{d}y.$$

Notice that damping effects have been taken into account in Eqs. (9)–(11). In the above equations, ξ_j is the modal damping ratio of the jth mode; Λ_j the jth modal factor of the cavity; M_n the nth modal mass of panels; and P_n^{IN} the amplitude of the nth modal pressure. J, N^I, and N^R are the number of acoustic and structural modes considered in the calculation. $C_{j,n}$ is the modal coupling coefficient characterizing the coupling strength between the nth structural mode and the jth acoustic mode.

The modal response of the incidence and radiation panels can be, respectively, solved from Eqs. (9) and (10) as

$$W_n^I=\frac{\sum_{h=1}^{J}C_{h,n}^I P_h-2P_n^{\mathrm{IN}}}{[\omega^2+\mathrm{i}2\xi_n^I\beta_n^I-(\beta_n^I)^2]M_n^I}, \tag{12}$$

$$W_n^R=-\frac{\sum_{h=1}^{J}C_{h,n}^R P_h}{[\omega^2+\mathrm{i}2\xi_n^R\beta_n^R\omega-(\beta_n^R)^2]M_n^R}. \tag{13}$$

Substituting Eqs. (12) and (13) into (11), a set of linear equations (j=1,2,…,J) with the amplitude of modal pressure responses as unknowns is obtained as follows:

$$\left\{(\alpha_j^2-\mathrm{i}2\xi_j^C\alpha_j\omega-\omega^2)\frac{\Lambda_j}{\rho_0c^2}+\sum_{m=1}^{M}\frac{\mathrm{i}\omega[\varphi_j(x_m^T,y_m^T,z_m^T)]^2}{Z_m}+\sum_{n=1}^{N^I}\frac{\omega^2(C_{j,n}^I)^2}{[\omega^2+\mathrm{i}2\xi_n^I\beta_n^I-(\beta_n^I)^2]M_n^I}+\frac{\omega^2(C_{j,n}^R)^2}{\left[\omega^2+\mathrm{i}2\xi_n^R\beta_n^R\omega-(\beta_n^R)^2\right]M_n^R}\right\}P_j,$$

$$\sum_{h\neq j}^{J}\left\{\sum_{m=1}^{M}\frac{\mathrm{i}\omega\varphi_j(x_m^T,y_m^T,z_m^T)\varphi_h(x_m^T,y_m^T,z_m^T)}{Z_m}+\sum_{n=1}^{N^I}\frac{\omega^2C_{j,n}^IC_{h,n}^I}{[\omega^2+\mathrm{i}2\xi_n^I\beta_n^I-(\beta_n^I)^2]M_n^I}+\sum_{n=1}^{N^R}\frac{\omega^2C_{j,n}^RC_{h,n}^R}{\left[\omega^2+\mathrm{i}2\xi_n^R\beta_n^R\omega-(\beta_n^R)^2\right]M_n^R}\right\}P_h=\sum_{n=1}^{N^I}\frac{2\omega^2C_{j,n}^IP_n^{\mathrm{IN}}}{\left[\omega^2+\mathrm{i}2\xi_n^I\beta_n^I-(\beta_n^I)^2\right]M_n^I}. \tag{14}$$

3. Simulations and measurements

In this section, the effectiveness of TARs in sound transmission control through a double-panel partition is investigated. To this end, a typical double-panel partition is used [2], which mainly consists of two identical glass panels divided by a rectangular cross-sectional spacer embedded with TARs. Panels and the spacer are bonded together and tightly held with a U-type aluminum frame. Notice that in each facing surface of the panels contacting with the spacer and U-type aluminum, a thin layer of soft silicon was used to prevent air leakage. Comparisons between the measured resonance frequencies and the theoretical calculations using a simply supported plate show that the maximum frequency difference is less than 3% in the range of [1, 400] Hz. Therefore, baffled simply supported panels are considered in the following simulations, while the above model is not restricted to this particular case. The dimensions and physical parameters associated with panels and cavity are tabulated in Table 1. Each T-shaped acoustic resonator used in simulations and experiments is denoted by "TAR_" followed by an integer corresponding to its working frequency. All resonators are designed using the formula shown in [5], and their dimensions are listed in Table 2.

A harmonic plane wave is supposed to impinge on the incidence panel at angles θ and ϕ [see Fig. 1(a)] with $p^{\mathrm{IN}}(x,y,z,t)=P^{\mathrm{IN}}e^{-\mathrm{i}(\omega t-k_xx-k_yy-k_zz)}$, where $k_x=k_0\sin\theta\cos\phi$, $k_y=k_0\sin\theta\sin\phi$, and $k_z=k_0\cos\theta$. The radiated pressure at the surface of the radiation panel can be computed using the formulation shown in [21] as

$$p_{\mathrm{rad}}(x,y,0)=\sum_{m=1}^{\infty}\sum_{n=1}^{\infty}V_m^RE_{m,n}^R\psi_n^R(x,y), \tag{15}$$

Table 1
Geometric dimensions and physical parameters of double-panel partition.

Parameters	Incidence panel	Radiation panel	Acoustic cavity
Length × width × thickness (mm)	830 × 830 × 3	830 × 830 × 3	830 × 830 × 19
Young's modulus (Pa)	60×10^9	60×10^9	–
Poisson ratio	0.22	0.22	–
Ambient temperature (°C)	–	–	20
Density (kg/m^3)	2373	2373	1.21
Sound speed (m/s)	–	–	343.6
Damping ratio	0.005	0.005	0.0028

Table 2
Dimensions of used TARs.

Resonator	Branch 1 diameter (mm)	Branches 2 & 3 width × height (mm)	L_{B1} (mm)	L_{B2} (mm)	L_{B3} (mm)
TAR_203	13.6	14.2 × 14.2	20	15	379.2
TAR_204	13.6	14.2 × 14.2	20	15	322.0
TAR_271	13.6	14.2 × 14.2	20	15	273.4
TAR_304	13.6	14.2 × 14.2	20	15	239.3
TAR_312	13.6	14.2 × 14.2	20	15	231.6
TAR_346	13.6	14.2 × 14.2	20	15	205.3

where $V_m^R = -\mathrm{i}\omega W_m^R$ is the mth modal velocity response of the radiation panel and $E_{m,n}^R$ is the modal radiation impedance of the panel, which is calculated by

$$E_{m,n}^R = \frac{c\rho_0}{2\pi}\int_{-\infty}^{\infty}\int_{-\infty}^{\infty} \Psi_m^R(k_x,k_y)\Psi_n^R(-k_x,-k_y)\frac{k_0}{\sqrt{k_0^2-k_x^2-k_y^2}}\,\mathrm{d}k_x\,\mathrm{d}k_y, \tag{16}$$

with $\boldsymbol{\Psi}_m^R(k_x,k_y)$ being the double Fourier transform of the mode shape $\psi_m^R(x,y)$ of the radiation panel, defined as

$$\boldsymbol{\Psi}_m^R(k_x,k_y) = \int_{-\infty}^{\infty}\int_{-\infty}^{\infty}\psi_m^R(x,y)\mathrm{e}^{\mathrm{i}(k_x x+k_y y)}\,\mathrm{d}x\,\mathrm{d}y = \iint_S \psi_m^R(x,y)\mathrm{e}^{\mathrm{i}(k_x x+k_y y)}\,\mathrm{d}x\,\mathrm{d}y.$$

Traditionally, the sound transmission loss (TL) is defined as the ratio of the incident power over the radiated power. Should this definition be used here, negative transmission loss could be observed at some plate resonances. This phenomenon can be explained by examining Eq. (1) for the incidence plate, where the sound pressure applied on the incidence plate is assumed as the blocked pressure, i.e., $2p^{\mathrm{IN}}$, where p^{IN} is the incident sound pressure. Although this is a widely accepted simplification, it has been shown by Guy [23,24] that the real pressure applied on the incidence plate is actually lower, depending on the mobility of the plate. The largest error occurs when the plate undergoes resonance with extremely low structural damping, both leading to an extremely high mobility of the panel. Therefore, the overestimated input pressure results in an overestimation of the transmitted power. Examples of negative sound transmission loss can be found in Ref [16]. Alternatively, in a large majority of works dealing with sound transmission loss of flexible plates [4,22–24], the TL is usually defined by directly using sound pressures. This definition is adopted in the present study as follows:

$$\mathrm{TL} = 10\log_{10}\frac{\langle (p^{\mathrm{IN}})^2\rangle}{\langle p_{\mathrm{rad}}^2\rangle}$$

where $\langle (p^{\mathrm{IN}})^2\rangle$ is the averaged incident sound pressure over the incidence panel and $\langle p_{\mathrm{rad}}^2\rangle$ is the averaged radiation sound pressure over the radiation panel. These quantities can be calculated by

$$\langle p^2\rangle = \frac{1}{2L_xL_y}\iint_S p(x,y,z_0)p^*(x,y,z_0)\,\mathrm{d}x\,\mathrm{d}y,$$

where the asterisk indicates the complex conjugate.

Substituting Eq.(15) into the above equation, $\langle p_{\mathrm{rad}}^2\rangle$ can be expressed as

$$\langle p_{\mathrm{rad}}^2\rangle = \frac{1}{2L_xL_y}(\mathbf{VE})\mathbf{D}(\mathbf{VE})^H = \frac{1}{8}\mathbf{P}_{\mathrm{rad}}\mathbf{P}_{\mathrm{rad}}^H \quad \text{(for simply supported plates)},$$

where $\mathbf{V}$ $(1\times M)$ is the modal velocity response vector of the plate, $\mathbf{E}$ $(M\times M)$ is the modal radiation impedance matrix, $\mathbf{D}$ (M × M) is the modal factor matrix of the plate whose diagonal elements are $d_{mm} = \iint_S[\psi_m^R(x,y)]^2\,\mathrm{d}x\,\mathrm{d}y$ and non-diagonal elements are zero, $\mathbf{P}_{\text{rad}}=\mathbf{VE}$, and H denotes the complex conjugate transpose. Preliminary study results show that the optimal locations of TAR are not sensitive to the incident angles. Therefore, in the following simulations, a plan wave TL is used to evaluate the effectiveness of TARs in the sound transmission control of double-panel partitions. It is worth noting that the negative TL based on this definition is possible due to the resonance effect of the system [23].

Convergence study of the TL is conducted in the frequency range of [1, 400] Hz, by gradually increasing the modal indices. The incident angles of the harmonic plane wave are set to $\theta=\pi/3$ and $\phi=\pi/6$ in all simulations. Upon a satisfactory convergence, a total of 64 acoustic cavity modes [$(l, m, n)=(0\text{–}7, 0\text{–}7, 0)$] and 64 structural modes [$(q, r)=(1\text{–}8, 1\text{–}8)$] are found to be sufficient. This will be used in the following simulations.

3.1. Characterization of sound transmission

The sound transmission through the double-panel partition is directly associated with the sound pressure distribution in the air cavity and the motion of the radiation panel. Incorporating acoustic resonators in a double-panel partition aims at reducing the sound pressure level inside the air cavity at the targeted frequencies, and thus attenuating pressures on the radiation panel to increase the TL. To provide a baseline for future analyses, the TL without resonators, the averaged sound pressure in the cavity, and the averaged quadratic velocity of the incidence and radiation panels are calculated. The averaged pressure in the cavity and the averaged quadratic velocity over the plate are, respectively, computed by [3]

$$\langle p^2 \rangle = \frac{1}{2L_xL_yh}\iiint_V p(x,y,z)p^*(x,y,z)\,\mathrm{d}x\,\mathrm{d}y\,\mathrm{d}z = \frac{1}{2L_xL_yh}\mathbf{P\Lambda P}^H, \tag{18}$$

$$\langle v^2 \rangle = \frac{1}{2L_xL_y}\iint_S vv^*\,\mathrm{d}x\,\mathrm{d}y = \frac{1}{2L_xL_y}\mathbf{VDV}^H, \tag{19}$$

where $\mathbf{P}$ is the modal pressure response vector in the cavity, and $\mathbf{\Lambda}$ is the modal factor matrix of cavity whose diagonal elements are Λ_j and non-diagonal elements are zero.

Calculation results are shown in Fig. 2, and the *in vacuo* natural frequencies of the panels and the natural frequencies of the rigid-walled air-cavity (see Table 3) are also indicated in the figure by dashed and solid vertical lines, respectively. Seven typical dips in TL curve, corresponding to the strong sound transmission, are identified and labeled in Fig. 2. On the basis of both coupled and uncoupled resonances of the panels and cavity, these dips are loosely classified into the following three categories: (1) acoustic-mode dominant (AMD): From the TL curve shown in Fig. 2(a), a marked dip (dip 3) is observed at 203 Hz. Modal decomposition analysis shows that the cavity modes of (0,0,0), (0,2,0), (2,0,0) and (2,2,0) significantly contribute to the sound pressure at this frequency, whose modal responses are 15–40 dB larger than those of other acoustic modes, including (0,1,0) and (1,0,0). Three of these dominant modes (0,2,0), (2,0,0) and (2,2,0) can induce large sound pressure at the mid-length point of the cavity, resulting in the pressure maximum there at 203 Hz. Therefore, strictly speaking, dip 3 at 203 Hz in the TL curve cannot be simply regarded as the mass–air–mass (MAM) resonance

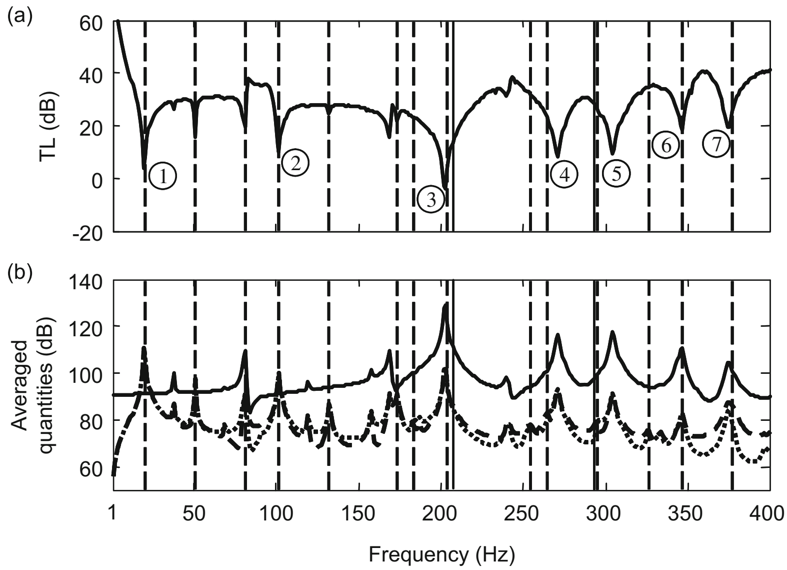

Fig. 2. Sound transmission characterization: (a) sound transmission loss and (b) (–) averaged sound pressure in cavity; (– –) averaged quadratic velocity of incidence panel; (· · · · · ·) averaged quadratic velocity of radiation panel.

Table 3
Natural frequencies and coupling factors.

Structural mode no.	Acoustic mode no.	(000)	(010)	(100)	(110)
	Natural freq. (Hz)	0	207	207	293
(11)	20	0.41	0	0	0
(12)	51	0	0.27	0	0
(21)	51	0	0	0.27	0
(22)	81	0	0	0	0.18
(13)	102	0.14	0	0	0
(31)	102	0.14	0	0	0
(23)	132	0	0	0.09	0
(32)	132	0	0.09	0	0
(14)	173	0	0.11	0	0
(41)	173	0	0	0.11	0
(33)	183	0.06	0	0	0
(24)	204	0	0	0	0.07
(42)	204	0	0	0	0.07
(34)	254	0	0.04	0	0
(43)	254	0	0	0.04	0
(15)	265	0.08	0	0	0
(51)	265	0.08	0	0	0
(25)	295	0	0	0.05	0
(52)	295	0	0.05	0	0
(44)	326	0	0	0	0.03
(35)	346	0.03	0	0	0
(53)	346	0.03	0	0	0
(16)	377	0	0.07	0	0
(61)	377	0	0	0.07	0

estimated at 231 Hz using unbounded, rigid double panel without damping [16,22]. In the current case, both plates undergo flexible motion at this frequency and involve significant contribution from higher order cavity modes. For convenience, this dip at 203 Hz is loosely called MAM and AMD dip. (2) Structural-mode dominant (SMD): SMD dips correspond to high structural resonance peaks, relatively distant from acoustic cavity resonances, and dominated by the structural resonances of the panels. In such categories are dips 1, 2, 6, and 7. (3) Coupled-mode dominant (CMD): CMD dips correspond to the newly emerged structural–acoustical resonance frequencies of the cavity response. These dips are strongly affected by the neighboring structural and acoustical modes. Therefore, their positions are not apparently tied with one particular uncoupled mode, either acoustic or structural. In the present case, dips 4 and 5 belong to this category.

The effectiveness of TARs is evaluated in terms of the three categories hereafter.

3.2. Control of AMD dips

A TAR_203 resonator is designed and incorporated in the double-panel partition to control the AMD dip at 203 Hz (dip 3). The optimal location of the TAR_203 is theoretically predicted and experimentally measured. Comparisons between the theoretical and experimental results are made.

The optimal location of the resonator is determined through comparing the computed TLs when varying the location of TAR along four edges of the air cavity between two panels. Staring from the corners, 43 locations along each edge are used in simulations. The predicted results are given in Fig. 3(a), which shows the predicted improvement of TL versus the variation of TAR location along x=10, 820 mm, y=10, and 820 mm. It is seen that better performance is achieved when the resonator is located at the middle of each edge. The largest TL improvement of 14.3 dB is achieved when TAR_203 was inserted at (820, 415, 9.5) mm. Fig. 3(b) shows the predicted sound pressure level (SPL) distribution at 203 Hz in the plane of z=9.5 mm in the cavity without resonators, and the optimal locations along each edge are also indicated with different symbols in the figure. Because of the dominance of the acoustic modes, the optimal locations match exactly with the maximum acoustic pressure location inside the cavity. The predicted TL through the double partition and the SPL at (800, 800, 9.5) mm are, respectively, shown in Figs. 4(a) and (b) when TAR_203 is inserted at (820, 415, 9.5) mm. The insertion of the single TAR results in a 13.9 dB reduction in SPL and an increase of 14.3 dB in TL at 203 Hz. Therefore, for the AMD dip, if only simply locating TARs at the maximum pressure areas inside the cavity, the SPL in the cavity can be significantly reduced, and further the TL through the double-panel partition can be well increased.

Experiments are conducted to verify the predicted optimal location of TAR_203. The fabricated partition is installed between an anechoic chamber and a reverberant chamber, as illustrated in Fig. 5. A loudspeaker driven by a white noise signal is located in the reverberant chamber and microphones are used to measure the autospectrum of sound pressures in the two sides of the partition. The noise reduction (NR) is used to experimentally determine the optimal location for the

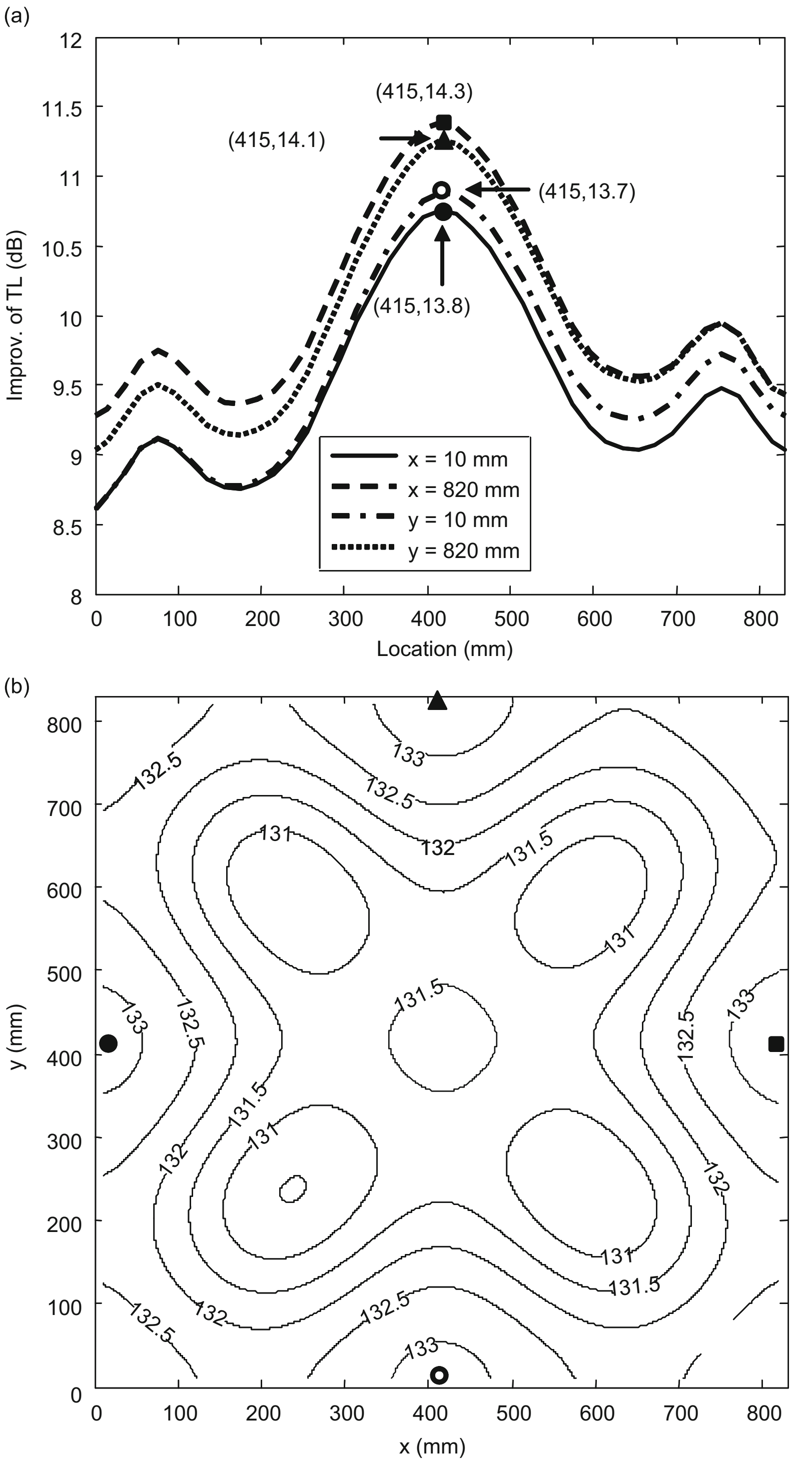

Fig. 3. (a) Predicted TL improvement with variation of resonator location along cavity edges and (b) SPL distribution at 203 Hz without TARs.

acoustic resonators. It is defined as

$$\mathrm{NR} = 10\log_{10}\frac{\langle p^2_{\text{incidence}}\rangle}{\langle p^2_{\text{radiation}}\rangle}$$

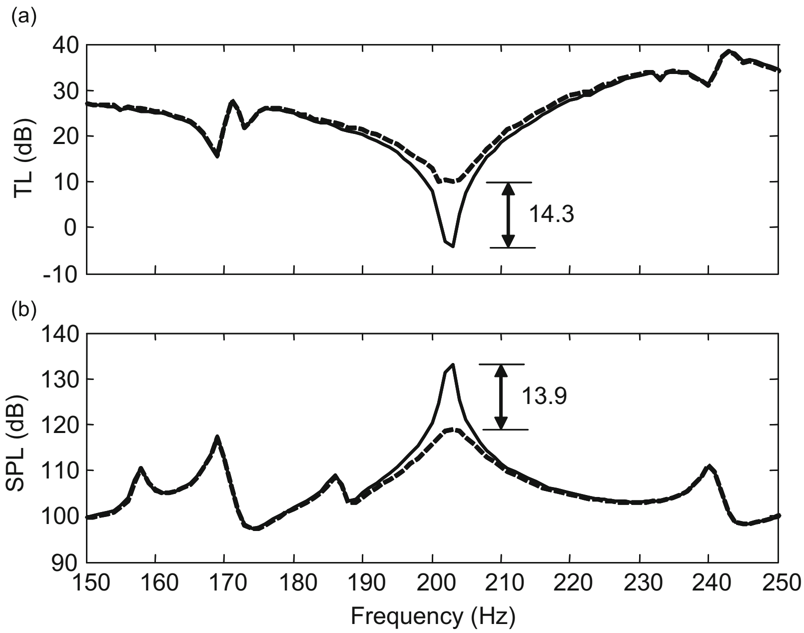

Fig. 4. Predicted results with (– –) and without (–) TAR_203.

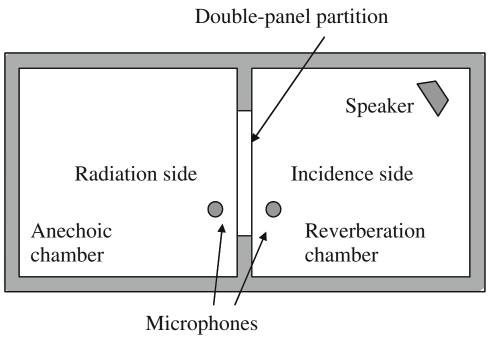

Fig. 5. Measurement setup.

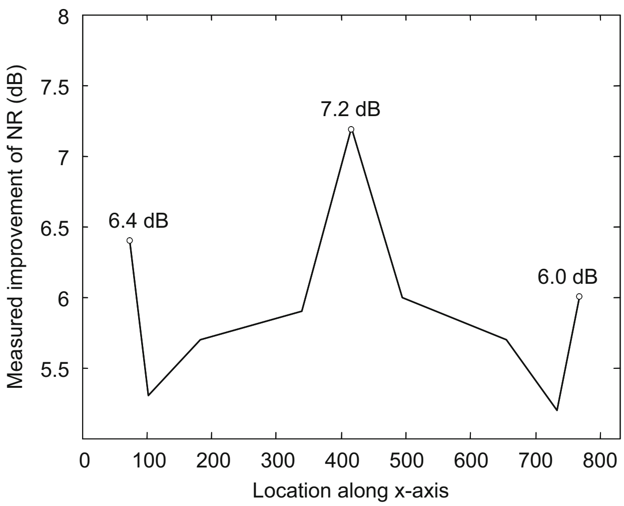

Fig. 6. Measured NR improvement as variation of resonator location along cavity edge.

where $\langle p^2_{\text{incidence}} \rangle$ is the measured sound pressure power spectrum in the incidence side averaged over the incidence panel and $\langle p^2_{\text{radiation}} \rangle$ is the measured sound pressure power spectrum in the radiation side averaged over the radiation panel. A TAR_204 was designed and fabricated (see Table 2). Notice that the frequency corresponding to the TL dip measured (204 Hz) slightly differs from that predicted (203 Hz). Similarly as in the simulation, the location of the TAR_204 is varied along the x-axis. Because of the practical difficulty in installing the resonator at the two ends near the corner, tests are carried out for nine locations from y=73 to 768 mm. The measured improvement in NR at different TAR locations is shown in Fig. 6. A maximum improvement of 7.2 dB in NR is achieved when the TAR_204 is located at (820, 415, 9.5) mm, which is exactly the same location as that predicted. Moreover, two smaller peaks measured at y=73 and 768 mm are consistent with the predicted two small peaks (at y=75 and 755 mm), corresponding to a 6.0–6.4 dB improvement in NR. When locating the TAR at the determined optimal location, the measured NR curves are shown in Fig. 7. It should be noted that two obvious coupled peaks can be observed in the measured NR curve after the TAR is inserted, while there are no apparent coupled peaks in the theoretical curve. Simulations show that the formula for computing γ_j proposed in [20] leads to a large attenuation coefficient for the TAR. It has been known that a heavily damped resonator can completely mask the two coupled peaks on each side of the Helmholtz resonance frequency of the TAR, resulting in the differences between the

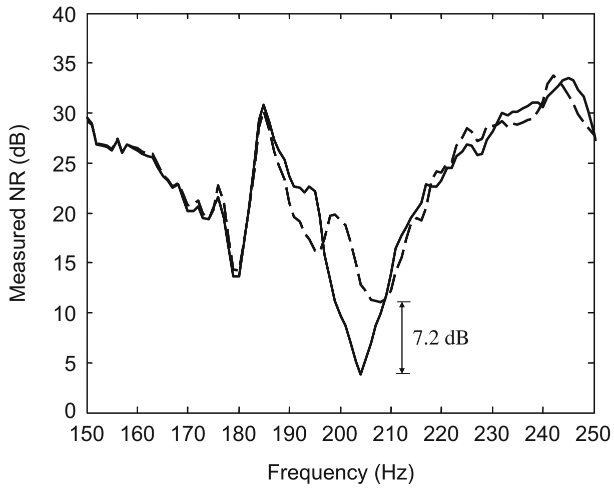

Fig. 7. Measured NR with (– –) and without (–) TAR_204.

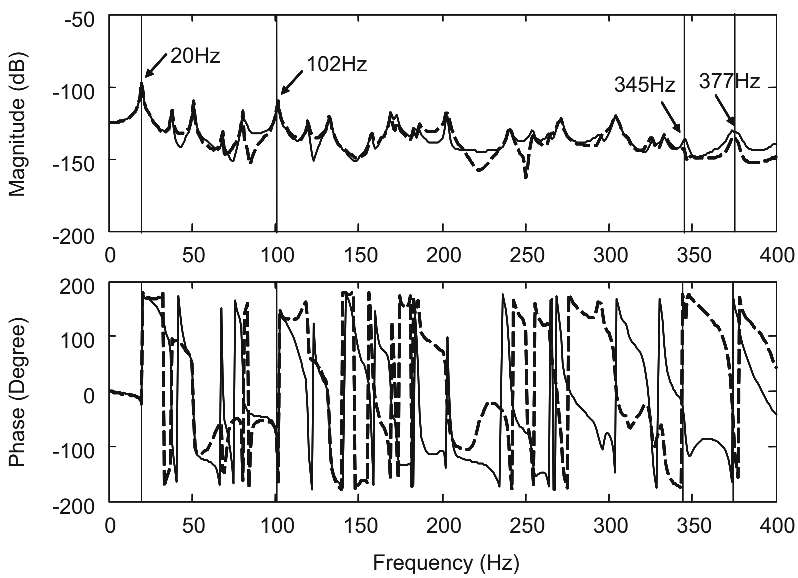

Fig. 8. Displacement of incidence (–) and radiation (– –) panels at (50, 50) mm.

two sets of results [25]. The predicted large attenuation coefficient overestimates the energy dissipation by the TAR and results in a better control performance than the measured one. Nevertheless, experimental results show that the theoretically predicted optimal location for the TAR is not affected by the estimation error of the attenuation coefficient γ_j.

3.3. Control of SMD dips

Three SMD dips, dips 1, 2, 6, and 7 involved in the present configuration, are investigated. Dip 1 is governed by the structural mode (1,1) at 20 Hz, dip 2 by modes (1,3) and (3,1) at 102 Hz, dip 6 by (3,5) and (5,3) at 346 Hz, and dip 7 by (1,6) and (6,1) at 375 Hz. Without loss of generality, the Bode plot of the displacement response at the arbitrary point (50, 50) mm on the incidence and radiation plates without resonators is shown in Fig. 8. It is observed that at 20 and 102 Hz, the two plates move in phase with the same amplitude. As expected, this in-phase motion of the panels does not result in any pressure rise in the sound pressure level inside the air cavity (not shown here), and simulations demonstrate that no control can be achieved by TARs for such modes.

On the contrary, for the SMD resonances at 346 Hz (dip 6) and 375 Hz (dip 7), the two plates move with different amplitudes and different phases, generating a pressure peak inside the cavity (see Figs. 2 and 8). In the following, only the

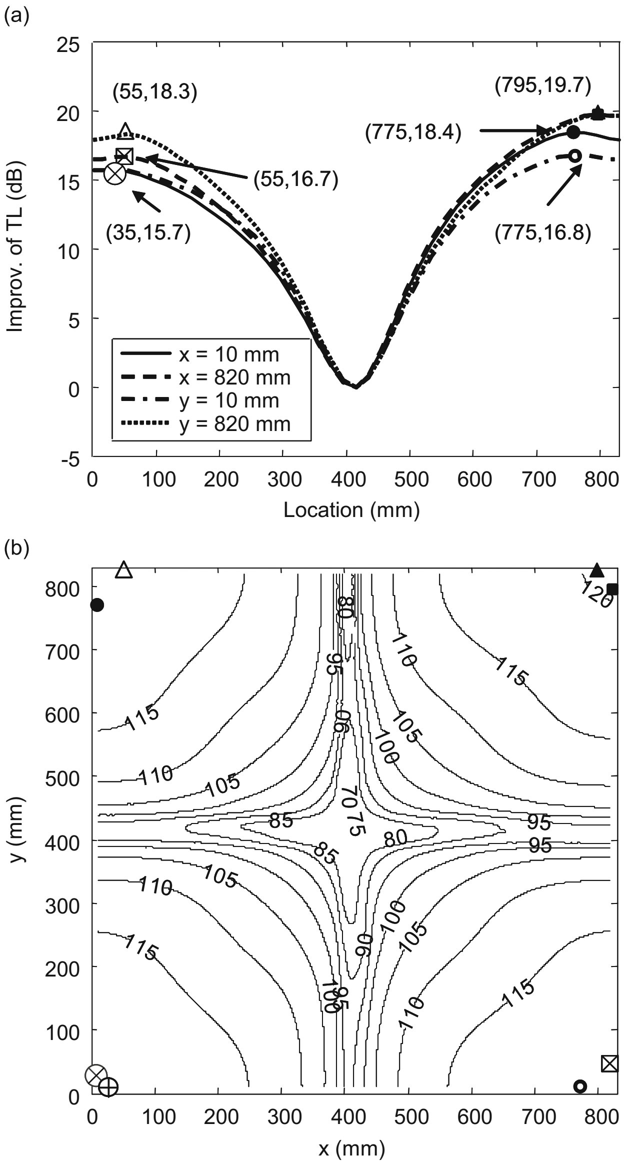

Fig. 9. (a) Predicted TL improvement as variation of resonator location along cavity edges and (b) SPL distribution at 346 Hz without TARs.

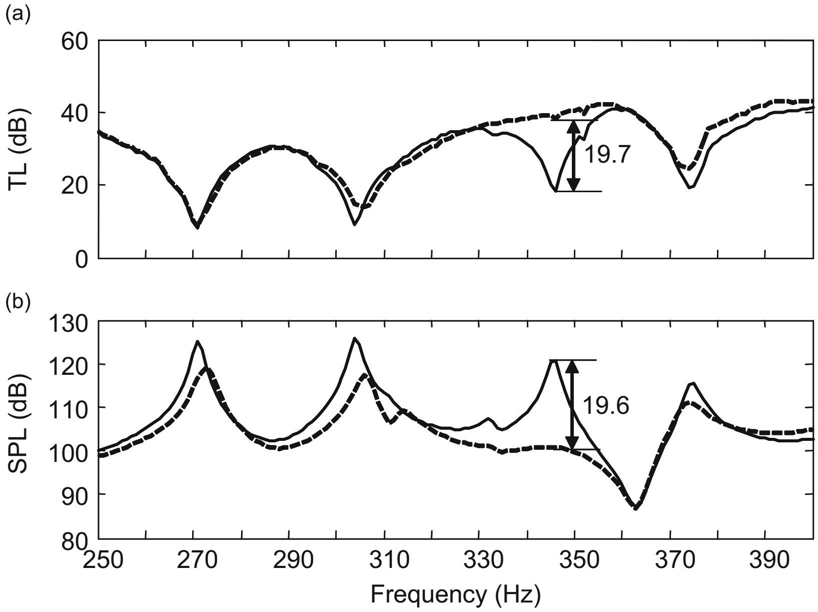

Fig. 10. Predicted results with (– –) and without (–) TAR_346.

control performance of the TAR at dip 6 is theoretically evaluated. The predicted TL improvement in the vicinity of 346 Hz is shown in Fig. 9(a) when the location of a TAR_346 is varied along the cavity edges. The SPL distribution in the mid z-plane inside the cavity without resonators is also shown in Fig. 9(b). It can be seen that good TL control can be achieved by locating TAR_346 in the high sound pressure areas, but not necessarily at the highest sound pressure locations. The largest increase of the TL is 19.7 dB when the resonator is located at (820, 795, 9.5) mm or (795, 820, 9.5) mm. The control results of TL and SPL at (800, 800, 9.5) mm in the cavity when the TAR is placed at (820, 795, 9.5) mm are shown in Fig. 10. The insertion of the single TAR_346 results in a 19.6 dB SPL reduction in the cavity and an increase of 19.7 dB in TL at 346 Hz.

3.4. Control of CMD dips

Dip 4 at 271 Hz and dip 5 at 304 Hz are dominated by newly emerged structural–acoustic modes. Using one TAR_271 with variable locations, the predicted TL improvement is illustrated in Fig. 11(a), which shows very limited improvement. A maximum of 1.4 dB increase in TL is achieved when the resonator is inserted at (820, 515, 9.5) mm, and accompanied by an 8.8 dB improvement in TL at 304 Hz. The reason for the improvement is explained as follows: When inserting a TAR into the cavity of a structural–acoustic coupled system, the resonator is coupled with all acoustic cavity modes as indicated by the resonator term $\sum_{h=1}[\varphi_j(x_m^T,y_m^T,z_m^T)\varphi_h(x_m^T,y_m^T,z_m^T)P_h/Z_m]$ in Eq. (11). After introducing the TAR, a new system is formed. Within the new system, the energy will be re-distributed among acoustic modes based on the fully coupled Eq. (11) since the old balance of the system has been disintegrated. Indeed, the modal pressure response at the targeted frequency is reduced as expected; however, the modal pressure responses in other nontargeted frequencies may be larger or smaller, corresponding to either an improved or worsened value in the TL curve. The distribution of SPL at 271 Hz in the plane z=9.5 mm inside the cavity without resonators is shown in Fig. 11(b). It is pertinent to mention that the optimal locations do not match with those locations having the maximum pressure.

Compared to that of dip 4, the control of dip 5 at 304 Hz proves to be much more successful as shown in Fig. 12. In fact, a 16.2 dB reduction in TL is achieved when a TAR_304 is positioned at (820, 595, 9.5) mm (see Fig. 13). Fig. 12(a) shows that the most significant improvement is obtained when the resonator moves along the two edges corresponding to x=10 and 820 mm. Surprisingly enough, the sound pressure level along these two edges is generally much lower than the other two edges (y=10 and 820 mm) as indicated by Fig. 12(b), which provides another testimony that the optimal location does not necessarily fall into the highest sound pressure areas.

The differences between the CMD dips 4 and 5 in terms of control performance may be attributed to the coupling nature of the system. In fact, multiple structural modes exist in the vicinity of 271 Hz, all being away from acoustic modes. This makes control difficult by using acoustic resonators. In order to further improve the sound transmission loss at 271 Hz, multiple acoustic resonators are needed (see Section 3.5). On the contrary, dip 5 is close to the uncoupled acoustic mode (1,1,0) at 293 Hz; therefore the sound response in the cavity can be effectively reduced by the acoustic resonator through coupling with the cavity mode (1,1,0), and thus the sound transmission loss at 304 Hz can be well improved just by one acoustic resonator. As a whole, simulated results suggest that CMD dips can be easily controlled if there are acoustic modes

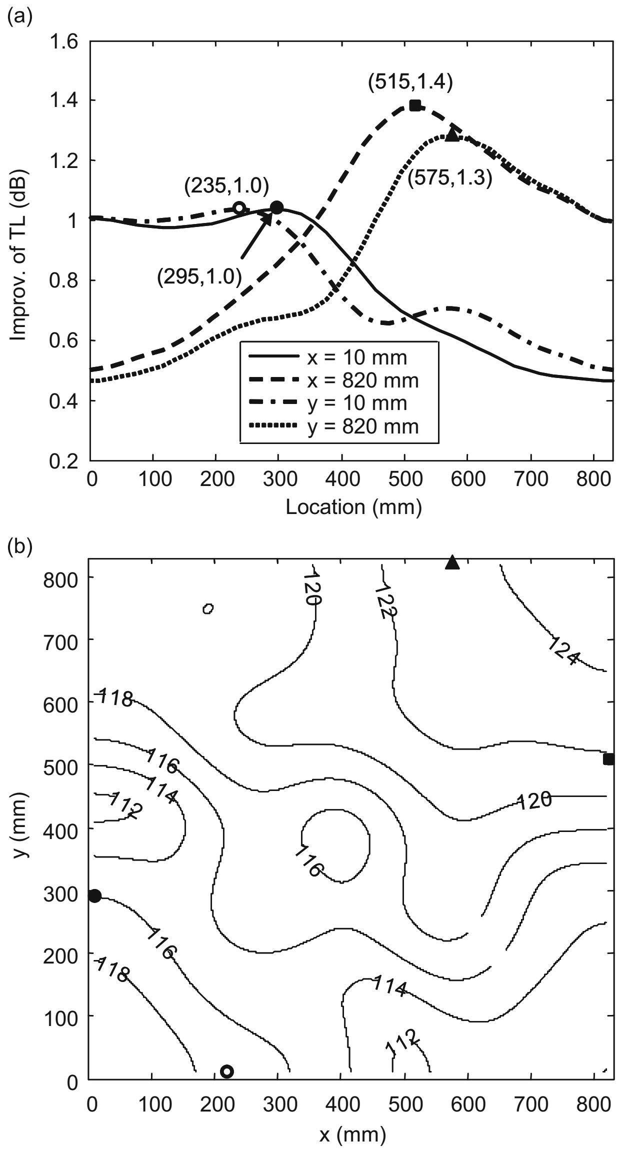

Fig. 11. (a) Predicted TL improvement as variation of resonator location along cavity edges and (b) SPL distribution at 271 Hz without TARs.

being involved in its vicinity. In all CMD cases, the determination of the optimal location of the resonator becomes more delicate. Not only the resonator can affect other frequencies in a very sensitive manner, but also the optimal location of the resonator is not always located at the highest sound pressure area.

Experiments are also conducted to verify the control performance in the CMD dip 5 at the measured resonance frequency of 312 Hz using a TAR_312. The fabricated TAR is installed in the predicted optimal location at (820, 595, 9.5) mm, and the measured NRs with and without the TAR are illustrated in Fig. 14. An 8.1 dB increase in NR is achieved, compared to 16.2 dB predicted by simulations. Again, this is probably resulted from the overestimated attenuation coefficient of the TAR as explained above.

3.5. Broadband control

The potential of multiple acoustic resonators in achieving broadband control is demonstrated here. Six TARs, including two TAR_203 and four TAR_271, are used. Based on the control result achieved in Sections 3.2 and 3.4, the two TAR_203 are installed at (10, 415, 9.5) mm and (820, 415, 9.5) mm, respectively; the four TAR_271 are positioned in the four corners of the air cavity. The predicted TL curves with and without resonators are shown in Fig. 15. It can be seen that two targeted

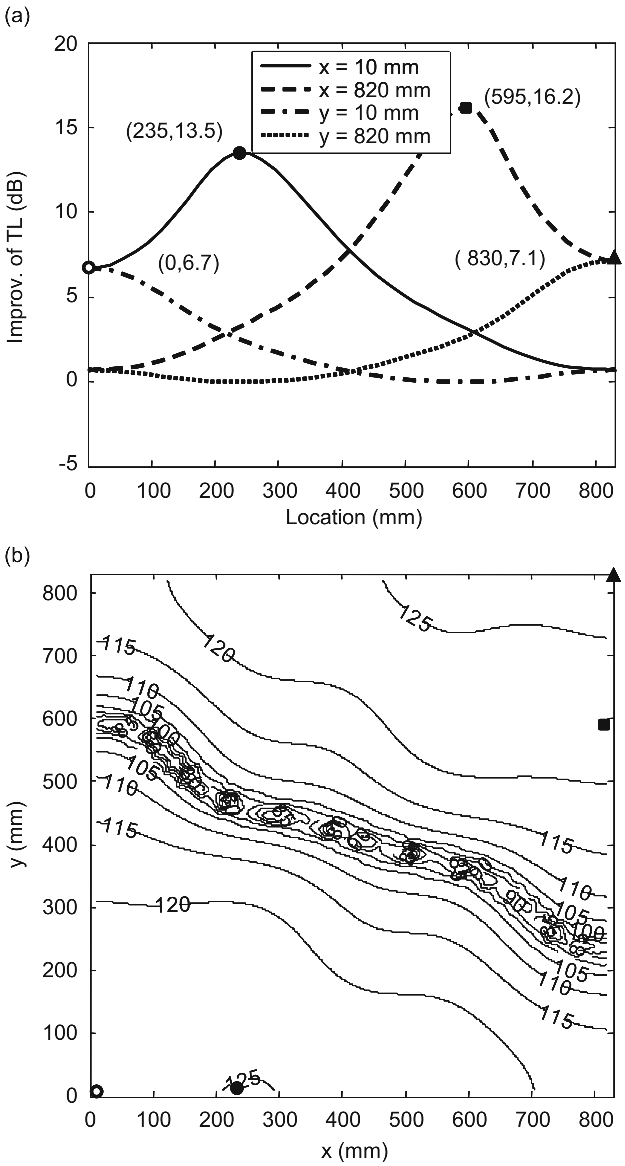

Fig. 12. (a) Predicted TL improvement as variation of resonator location along cavity edges and (b) SPL distribution at 304 Hz without TARs.

dips at 203 and 271 Hz are increased by 20.3 and 10.5 dB, respectively, and other two nontargeted dips at 304 and 346 Hz are also, respectively, improved by 16.1 and 18.6 dB due to the strong structural and acoustic coupling. Therefore, at the expense of adding more resonators, significant broadband control can be achieved.

4. Discussion and conclusion

A double-panel partition having inherent noise insulation capability at low frequencies is proposed. A general model, simulating sound transmission through the double-panel partition system with integrated T-shaped acoustic resonators, is developed. On the basis of both coupled and uncoupled resonances of the panels and cavity, the sound transmission through the double-panel partition is categorized and characterized. The effectiveness of the acoustic resonator in sound transmission control is examined based on the coupling nature of the system. Finally, a broadband sound transmission control is illustrated by using six TARs.

It is shown that, by means of reducing sound pressure level in the air cavity, TARs can well enhance the sound transmission loss of the double-panel partitions at most frequencies where conventional double partitions fail,

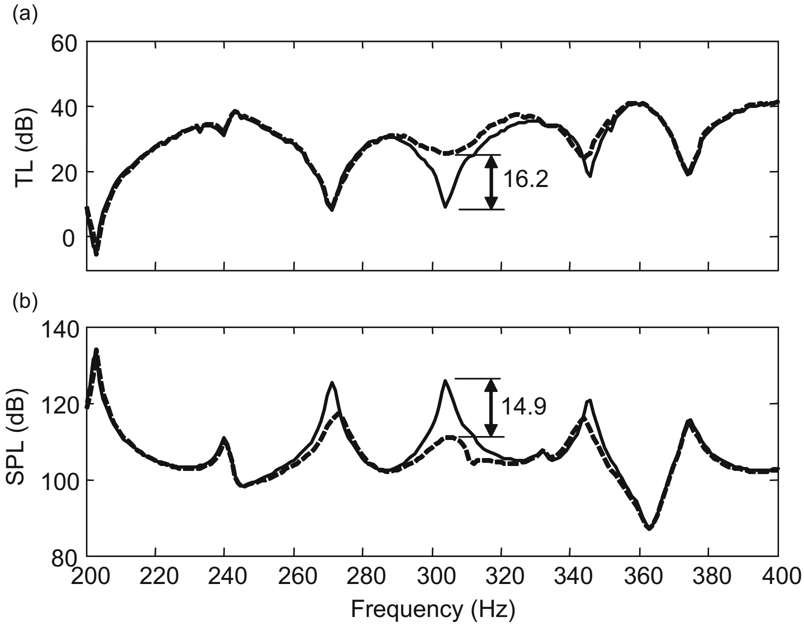

Fig. 13. Predicted results with (– –) and without (–) TAR_304.

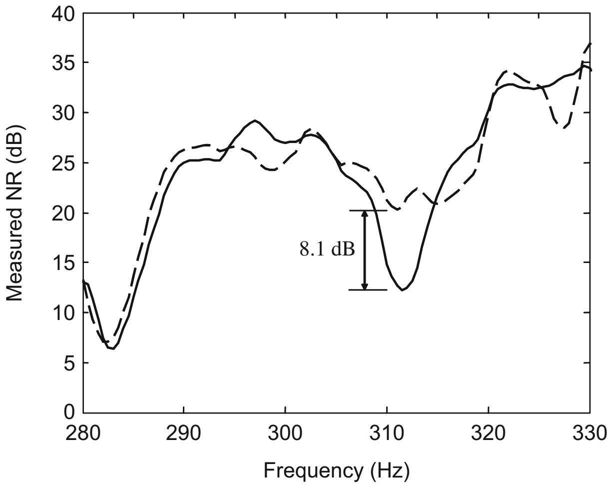

Fig. 14. Measured NR with (– –) and without (–) TAR_312.

corresponding to the dips appearing in the TL curves. These dips are classified into three categories: acoustic-mode dominant (AMD), structural-mode dominant (SMD), and coupled-mode dominant (CMD). For AMD dips, the sound transmission loss can be significantly improved using TARs. In this case, TARs can simply be located at the maximum pressure areas inside the air gap between the panels. When the sound transmission is governed by SMD modes, resulting in a pressure peak in the cavity, the sound transmission loss can also be significantly improved by TARs. In addition, the optimal location of the resonator, which does not always match with the maximum pressure area, must be carefully determined using the current model. However, when the two panels undergo in-phased motion with equal amplitude, the effect of the TAR is completely neutralized. When the sound transmission is dominated by CMD modes, better control can be achieved if there exist acoustic modes in the vicinity of the frequency of interest. In all CMD cases, the optimal location of the resonator needs to be meticulously determined. Not only the resonator can affect nontargeted frequencies in a very sensitive manner, but also the optimal location of the resonator may not be located at the highest sound pressure area, in which cases a simulation tool as the present one becomes indispensable.

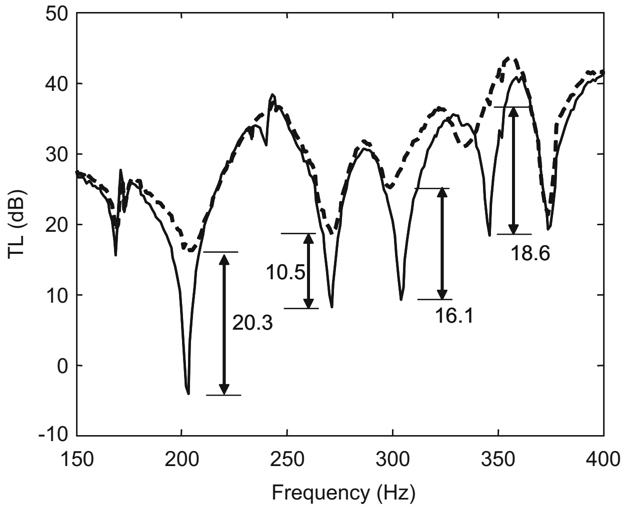

Fig. 15. Predicted results with (– –) and without (–) six TARs.

Acknowledgements

The authors wish to acknowledge support from Research Grants Council (project no. PolyU 5137/06E) and Innovation and Technology Commission (ITS062/09) of Hong Kong SAR.

References

[1] J.D. Quirt, Sound transmission through windows I. Single and double glazing, *Journal of the Acoustical Society of America* 72 (1982) 834–845.
[2] J.D. Quirt, Sound transmission through windows II. Double and triple glazing, *Journal of the Acoustical Society of America* 74 (1983) 534–542.
[3] L. Cheng, Y.Y. Li, J.X. Gao, Energy transmission in a mechanically-linked double-wall structure coupled to an acoustic enclosure, *Journal of the Acoustical Society of America* 117 (2005) 2742–2751.
[4] J.M. Mason, F.J. Fahy, The use of acoustically tuned resonators to improve the sound transmission loss of double-panel partitions, *Journal of Sound and Vibration* 124 (1988) 367–379.
[5] D. Li, J.S. Vipperman, On the design of long T-shaped acoustic resonators, *Journal of the Acoustical Society of America* 116 (2004) 2785–2792.
[6] D. Li, J.S. Vipperman, Noise control of a chambercore payload fairing using integrated acoustic resonators, *Journal of Spacecraft and Rockets* 43 (2006) 877–882.
[7] C. Bao, J. Pan, Experimental study of different approaches for active control of sound transmission through double walls, *Journal of the Acoustical Society of America* 102 (1997) 1664–1670.
[8] X. Pan, T.J. Sutton, S.J. Elliott, Active control of sound transmission through a double-leaf partition by volume velocity cancellation, *Journal of the Acoustical Society of America* 104 (1998) 2828–2835.
[9] J.P. Carneal, C.R. Fuller, An analytical and experimental investigation of active structural acoustic control of sound transmission through double panel systems, *Journal of Sound and Vibration* 272 (2004) 749–771.
[10] A. London, Transmission of reverberant sound through double walls, *Journal of the Acoustical Society of America* 22 (1950) 270–279.
[11] A.J. Price, M.J. Crocker, Sound transmission through double panels using statistical energy analysis, *Journal of the Acoustical Society of America* 47 (1970) 683–693.
[12] F.C. Sgard, N. Atalla, J. Nicolas, A numerical model for the low frequency diffuse field sound transmission loss of double-wall sound barriers with elastic porous linings, *Journal of the Acoustical Society of America* 108 (2000) 2865–2872.
[13] J.D. Chazot, J.L. Guyader, Prediction of transmission loss of double panels with a path-mobility method, *Journal of the Acoustical Society of America* 121 (2007) 267–278.
[14] S.J. Estève, M.E. Johnson, Reduction of sound transmitted into a circular cylindrical shell using distributed vibration absorbers and Helmholtz resonators, *Journal of the Acoustical Society of America* 112 (2002) 2840–2848.
[15] S.J. Estève, M.E. Johnson, Reduction of sound transmitted into a composite cylinder using distributed vibration absorbers and Helmholtz resonators, *Journal of Vibration and Acoustics* 112 (2002) 2040–2048.
[16] Q. Mao, S. Pietrzko, Control of sound transmission through double wall partitions using optimally tuned Helmholtz resonators, *Acta Acoustica* 91 (2005) 723–731.
[17] D. Li, L. Cheng, G.H. Yu, J.S. Vipperman, Noise control in enclosures: modeling and experiments with T-shaped acoustic resonators, *Journal of the Acoustical Society of America* 122 (2007) 2615–2625.
[18] J.L. Guyader, B. Laulagnet, Structural acoustic radiation prediction: expanding the vibratory response on a functional basis, *Applied Acoustics* 43 (1994) 247–269.
[19] L.E. Kinsler, A.R. Frey, A.B. Coppens, J.V. Sanders, Fundamentals of Acoustics, third ed., John Wiley & Sons, New York, 1982.
[20] D. Pierce, *Acoustics: An Introduction to its Physical Principles and Applications*, Acoustical Society of America, 1989.
[21] E.C. Sewell, Transmission of reverberant sound through a single-leaf partition surrounded by an infinite rigid baffle, *Journal of Sound and Vibration* 12 (1970) 21–32.
[22] F.J. Fahy, P. Gardonio, Sound and Structural Vibration: Radiation, Transmission and Response, second ed., Academic Press in an imprint of Elsevier, 2007.
[23] R.W. Guy, M.C. Bhattacharya, The transmission of sound through a cavity-backed finite plate, *Journal of Sound and Vibration* 27 (1973) 207–223.
[24] R.W. Guy, A.J. Pretlove, Cavity-backed panel resonance, *Journal of Sound and Vibration* 27 (1973) 128–129.
[25] G.H. Yu, D. Li, L. Cheng, Effect of internal resistance of a Helmholtz resonator on acoustic energy reduction in enclosures, *Journal of the Acoustical Society of America* 124 (2008) 3534–3543.